Effective Proton Heating through Collisionless Driven Reconnection in the Presence of Guide Field*)

Shunsuke USAMI[1)], Ritoku HORIUCHI[1,2)], Hiroaki OHTANI[1,2)], Yasushi ONO[3)] and Hiroshi TANABE[3)]

[1)]*National Institute for Fusion Science, National Institutes of Natural Sciences, Toki 509-5292, Japan*
[2)]*Sokendai (The Graduate University of Advanced Studies), Toki 509-5292, Japan*
[3)]*University of Tokyo, Tokyo 113-8654, Japan*

(Received 28 December 2017 / Accepted 27 February 2018)

The plasma heating mechanism during magnetic reconnection in the presence of guide magnetic field is investigated by means of particle simulations and test particle simulations. Particle simulations demonstrate that ring-like structures of ion velocity distributions are formed in the downstream, where a large percentage of ions are effectively heated. Furthermore, a single ion motion is focused upon by using test particle simulations. The ion moves in the downstream direction owing to the $E \times B$ drift while in gyromotion. Finally, it is reported that the profile of the ion temperature obtained by the particle simulation fits well with the profile observed in the TS-3 experiment.

Keywords: particle simulation, magnetic reconnection, plasma heating, spherical tokamak, PASMO, TS-3

DOI: 10.1585/pfr.13.3401025

1. Introduction

It is widely believed that magnetic reconnection plays an important role in explosive activities such as sawtooth disruptions in a tokamak, solar flares, and geomagnetospheric substorms. In addition, magnetic reconnection has the interesting aspect that energy stored in the magnetic field is rapidly converted to particle kinetic and thermal energies. Plasma heating during magnetic reconnection is observed in laboratory plasmas such as in TS-3 and TS-4 at the University of Tokyo [1, 2], in MRX at the Princeton Plasma Physics Laboratory [3], and in MAST at the Culham Centre for Fusion Energy [4].

In this work, we address this important issue of magnetic reconnection, that is, the heating mechanism of ions (protons). For this purpose, we use tools of particle simulation and test particle simulation based on the particle simulation, since kinetic physics originating from nongyrotropic motions of plasma particles, which can not be treated by fluid models, play predominant roles in the heating process.

The paper is organized as follows. In Sec. 2, we highlight particle simulation results and briefly review how ions are effectively heated in the downstream. In Sec. 3, we focus on the motion of an ion particle by means of test particle simulations. In Sec. 4, we compare our simulation results with results reported in TS-3 experiments. Section 5 provides a summary of this work.

author's e-mail: usami.shunsuke@nifs.ac.jp

*) This article is based on the presentation at the 26th International Toki Conference (ITC26).

2. Review of the Effective Heating Process

Let us review the mechanism of the ion effective heating [5]. In order to study the mechanism of ion heating, we have carried out two-dimensional particle simulations by using the PASMO code [6, 7]. Figure 1 is the schematic diagram of plasma merging experiments in a spherical tokamak (ST) device. The simulation model by the PASMO mimics the boxed area drawn by the dotted line, which is the region near the contact point of the merging torus plasmas in an ST device, because the model implements the following features of plasma merging experiments in STs. First, the guide (toroidal) magnetic field exists as Horiuchi and Sato first applied [8]. That is, as the initial condition, we take a one-dimensional Harris-type equilibrium with a uniform guide field as $B_x(y) = B_{x0}\tanh(y/L)$ and $B_z(y) = B_{z0}$ for the magnetic field and $P(y) = P_0 + B_{x0}^2/(8\pi)\mathrm{sech}^2(y/L)$ for the plasma pressure, where B_{x0}, B_{z0}, and P_0 are constants and L is the spatial scale. Here, the ST device is displayed in the Fig. 1 by using the (R, Z) coordinate, which corresponds to the (x, y) coordinate used in the PASMO simulations. Next, plasmas are pushed by the driving electric field imposed on the upstream boundary in order to express plasmas pushed by the poloidal field coil current in experiments. On the other hand, the downstream boundary is free. Finally, the simulation domain covers the kinetic region including the contact point (the reconnection point).

The parameters of the particle simulation are as follows. The simulation domain size is $10.54(c/\omega_{\mathrm{pi}}) \times$

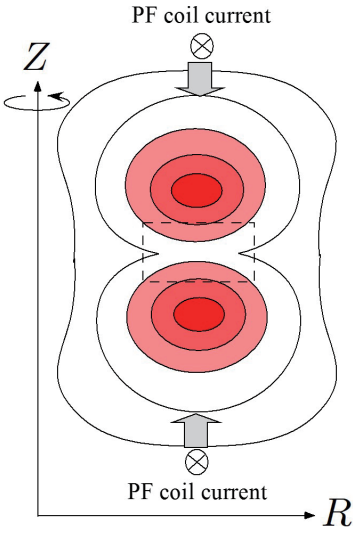

Fig. 1 Schematic diagram of a plasma merging experiment in a spherical tokamak (ST) device. The boxed area drawn by the dotted line is assumed to be simulated by the PASMO. The (R, Z) plane in the ST device corresponds to the (x, y) plane in the simulation.

$2.63(c/\omega_{\rm pi})$, where c is the speed of light and $\omega_{\rm pi}$ is the ion plasma frequency. The initial number of particles (electrons and ions) is 14,090,240. The ion-to-electron mass ratio is $m_{\rm i}/m_{\rm e} = 100$. The ratio of the electron plasma frequency to the electron gyrofrequency is $\omega_{\rm pe}/\omega_{\rm ce} = 6.0$. The Alfvén speed is $v_{\rm A}/c = 0.037$. The time step is $\omega_{\rm pi}\Delta t = 0.0052$, and the grid spacing is $\Delta_{\rm g}/(c/\omega_{\rm pi}) = 0.010$.

As described above, let us note that the reduced ion-to-electron mass ratio $m_{\rm i}/m_{\rm e} = 100$ is employed because of limited computer resources such as memory and CPU time. It is known that the global structure of magnetic reconnection does not depend on $m_{\rm i}/m_{\rm e}$. In contrast, the formation of the separatrix is associated with the electrostatic field originating from the charge separation. Thus, the width of the separatrix δ changes depending on $m_{\rm i}/m_{\rm e}$. The process of the ion effective heating described in this paper requires that ions are nonadiabatic across the separatrix. This condition is expressed as $\delta < \rho_{\rm i}$, which is satisfied in the simulations, where $\rho_{\rm i}$ is the ion Larmor radius. According to Guo *et al.* [9], it is estimated that $\delta \propto (m_{\rm i}/m_{\rm e})^{(1/4)}$. The ion Larmor radius is $\rho_{\rm i} \propto (m_{\rm i}/m_{\rm e})^{(1/2)}$ because the ion thermal velocity is $v_{\rm Ti} \propto (m_{\rm i}/m_{\rm e})^{(-1/2)}$, assuming that the electron temperature is equal to the ion temperature. Thus, $\delta < \rho_{\rm i}$ is better satisfied for the real ion-to-electron mass ratio $m_{\rm i}/m_{\rm e}$.

We show simulation results in the case of $B_{z0}/B_{x0} = 2$, $L/(c/\omega_{\rm pi}) = 0.66$, and $P_0/(B_{x0}^2/8\pi) = 0.35$. In Fig. 2, we show the spatial profiles of the magnetic field lines and the ion temperature perpendicular to the magnetic field as the color contours in the (x, y) plane at $\omega_{\rm pi}t = 780$. Magnetic reconnection is driven at almost the center of the simulation domain, and the ion temperature grows mainly in the

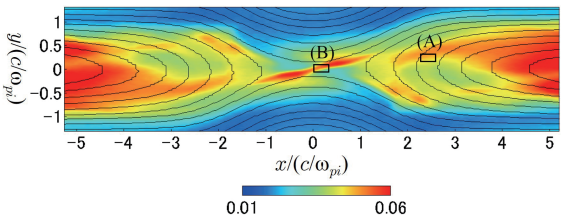

Fig. 2 Spatial profiles of the ion temperature perpendicular to the magnetic field (the color contours) and the magnetic field lines. The ion temperature rises mainly in the downstream.

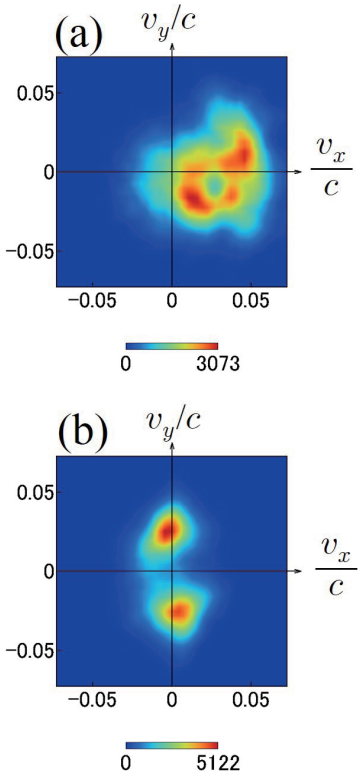

Fig. 3 Ion velocity distributions in the boxed areas (A) and (B) of Fig. 2. The panel (a) shows a ring-like structure and the panel (b) displays a two-peak structure.

downstream. In order to investigate the ion heating mechanism, we observe ion velocity distributions in the downstream. In Fig. 3 (a), we show an ion velocity distribution integrated over the boxed area (A) of Fig. 2. The ring-like structure of the velocity distribution is formed. That is, the distribution spreads [5]. In addition, Fig. 3 (a) indicates that a large percentage of ions are effectively heated in the downstream. Here it can be generally said that the main component ion in a plasma is responsible for the effective heating mechanism. In the simulation, the ions are usually regarded as protons. However, we can regard the ions as heavy ions so that the simulation mimics an experiment in which heavy ion plasmas such as helium ions are used.

The formation process of the ring-like velocity distribution, i.e., the mechanism of the ion effective heating is

explained as follows. We consider behaviors of ions entering the downstream across the separatrix from the upstream. In some cases, ions behave as nonadiabatic [10]. Upon crossing the separatrix, the electromagnetic field which ions feel rapidly changes. In addition, the ions do not gain enough kinetic energy from the electrostatic field on the separatrix, and thus the ion entry speed is much lower than the outflow speed. Now we take the following ideal case in order to avoid complicated considerations. In the downstream, the electromagnetic field is uniform and consists of the out-of-plane magnetic field B_z and the electric field perpendicular to the magnetic field E_y. Assuming that an ion with the initial velocity $\boldsymbol{v} = \mathbf{0}$ is located in the downstream, let us calculate the motion of the ion. The ion moves in the x direction with the velocity $v_x = cE_y/B_z$ (the $E \times B$ drift) while rotating around B_z with the speed cE_y/B_z (the gyromotion). The ion orbit is drawn as a cycloid. In the velocity space, the orbit is a circle whose center is $(cE_y/B_z, 0)$ and whose radius is cE_y/B_z. The ring-like structure of the velocity distribution is formed by such ions with different phases of the gyromotion.

3. Motion of an Ion Particle

We investigate motions of ion particles responsible for this effective heating process by means of test particle simulations. The equations of motion for test ion particles are calculated in the electromagnetic field given by the PASMO simulation. It is confirmed that magnetic reconnection is under the quasi-steady state, and the electromagnetic field does not significantly vary with time.

We plot the orbit, velocity, and kinetic energy of a typical ion particle responsible for the formation of the ring-like velocity distribution. The initial position of the test ion is taken to be on the upper upstream boundary $(x, y) = (1.37, 1.31)(c/\omega_{\rm pi})$. The ion has the initial velocity $(v_x, v_y) = (0.00663, -0.0124)c$, which is equal to the ion fluid velocity at the local position. For distinguishing the time in the test particle simulation from the time in particle simulations by the PASMO code, we use τ as the time in the test particle simulation. Figure 4 (a) shows the orbit of the ion particle, where the color contours indicate the electric field E_y. After the ion enters the downstream at $\omega_{\rm pi}\tau \simeq 60$, it returns to the separatrix, gyrates once inside the separatrix region, and then enters the downstream at $\omega_{\rm pi}\tau \simeq 100$ again [11]. After the re-entry to the downstream, this ion moves in the x direction with oscillating. The orbit is drawn as a cycloid-like curve due to the gyromotion and the $E \times B$ drift as described in Sec. 2.

In Fig. 4 (b), we plot the ion orbit in the velocity space (v_x, v_y). The part $\omega_{\rm pi}\tau \simeq 60 - 100$ of the first small circle indicates the gyromotion inside the separatrix region. The next circle ($\omega_{\rm pi}\tau \simeq 140 - 200$) corresponds to the gyromotion and the $E \times B$ drift in the downstream. In Sec. 2, the electromagnetic field is assumed to be uniform. In actual simulations as shown by the color contours in Fig. 4 (a), the

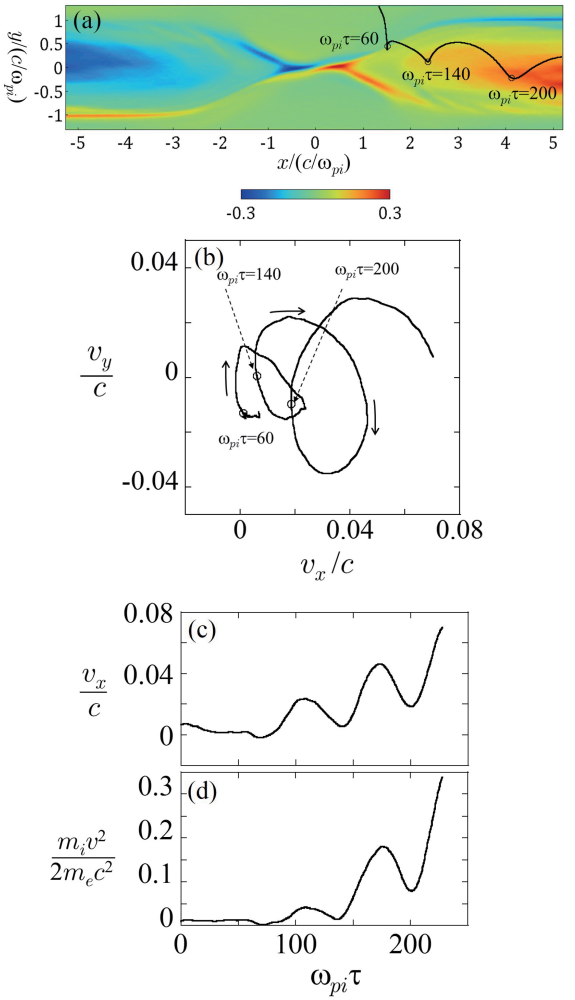

Fig. 4 Motion of an ion particle calculated by a test particle simulation. The panels (a), (b), (c), and (d) depict the orbit in the (x, y) plane, the orbit in the (v_x, v_y) plane, the time evolution of v_x, and time evolution of the kinetic energy, respectively.

electric field, however, is observed to become larger in the deeper downstream (as x is larger). Thus, the radius of the velocity circle becomes larger and the center of the circle moves in the v_x direction.

Figure 4 (c) demonstrates the time evolution of v_x. At $\omega_{\rm pi}\tau \simeq 140$, when the ion is in the downstream, v_x is much smaller than the outflow speed $u_{\rm out} \simeq 0.03c$. The velocity v_x rapidly increases because the increment in v_y caused by the E_y acceleration transforms to the increment in v_x owing to the gyromotion.

Lastly, we plot the time development of the kinetic energy of the ion in Fig. 4 (d). At $\omega_{\rm pi}\tau \simeq 140$, the kinetic energy can be regarded as almost zero. We can find that the ion gains kinetic energy in the downstream. If the electromagnetic field were uniform, the kinetic energy would return to zero (the value at $\omega_{\rm pi}\tau \simeq 140$) after the one gyration. However, the electric field becomes higher in the deeper downstream, and thus the ion does not lose all the kinetic energy after the one gyration.

4. Comparison with Experimental Results

In this section, we compare the ion temperature obtained by PASMO simulations with the ion temperature observed by TS-3 experiments. It is noted that in Fig. 5 the temperature is normalized to the initial ion temperature in the upstream T_{i0} and the length is normalized to the ion Larmor radius ρ_i, where ρ_i is defined by using the initial thermal speed and the initial reconnecting field.

As simulation results, in Figs. 5 (a) - (c) we display the x-axis profiles of the ion temperature perpendicular to the magnetic field along $y = 0$. The x-axis is in the downstream direction. In the case of $B_{z0}/B_{x0} = 2$ as shown in Fig. 5 (a), the ion temperature is increased in the downstream. In addition, we can see that the profile has a sharp peak in the vicinity of the reconnection point ($x = 0$). This is an apparent increment in the temperature originating from the meandering motion of ions [12]. The ion velocity distribution in the vicinity of the reconnection point (the boxed area (B) of Fig. 2) is shown in Fig. 3 (b). There are two peaks in the distribution. This is because nongyrotropic ions move back and forth across the reconnection point. In the simulations, we define the temperature as $m_i\langle v - \langle v\rangle\rangle^2$, where v is the velocity of a particle locating at a local point and $\langle\rangle$ denotes the ensemble average. Therefore, the two-peak structure in the velocity distribution leads to the apparent rising of the temperature. In contrast, in the cases of larger guide fields as shown in Figs. 5 (b) and (c), the apparent rising of the temperature at the reconnection point becomes unclear. It would also be a quite interesting and important topic to clarify what mechanism causes the apparent temperature increment depending on the strength of the guide field. However, this issue is beyond this work and thus is not discussed in this paper, but will be discussed in the future paper.

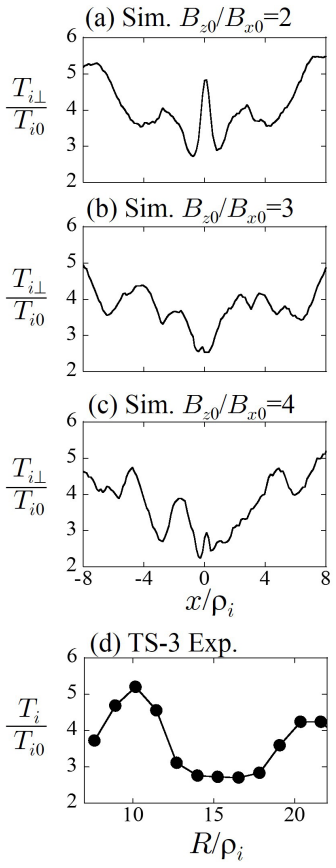

Fig. 5 Profiles of the ion temperature. The panels (a) - (c) are obtained by the PASMO and the panel (d) is observed by the TS-3 experiment.

Figure 5 (d) shows the radial profile of the ion temperature on the mid-plane observed by the TS-3 experiment [2], in which the ratio of the guide field to the reconnecting field is $\simeq 5$. The R-axis is in the downstream direction. Here, we estimate that $\rho_i \simeq 1.1$ cm and $T_{i0} \simeq 10$ eV.

Comparing Figs. 5 (c) and (d), we can see that the profiles are in agreement with each other. Described quantitatively, both profiles demonstrate that the temperature near the reconnection point is 2 - 3 times higher than the initial temperature and the temperature in the downstream is 4 - 5 times higher than the initial temperature.

5. Summary

By means of particle simulations we have studied the proton heating mechanism during magnetic reconnection in the presence of guide magnetic field. It has been found that the ion temperature rises mainly in the downstream, where ring-like structures of ion velocity distributions are formed. A large percentage of ions are effectively heated in the downstream. We have carried out test particle simulations and investigated the motion of a single particle of the ions effectively heated. It has been confirmed that the ion particle rotates around the out-of-plane magnetic field and moves in the outflow direction owing to the $E \times B$ drift. Lastly, we have compared the ion temperature profiles obtained by our particle simulations and by the TS-3 experiment. The profile in the simulation case of the high guide field is similar to the profile in the experiment.

Acknowledgments

This simulation work was performed on "Plasma Simulator" (FUJITSU FX100) at the National Institute for Fusion Science. This work was partially supported by a Grant-in-Aid for Scientific Research from the Japan Society for the Promotion of Science (Grant No. 16K17847), the Research Cooperation Program on "Hierarchy and Holism in Natural Sciences" and "Magnetic Reconnection Studies with Kinetic Simulations" at the National Institutes of Natural Sciences, the General Coordinated Research at the National Institute for Fusion Science (NIFS17KNTS049, NIFS17KNSS085), and "Joint Usage/Research Center for Interdisciplinary Large-scale Information Infrastructures" and "High Performance Computing Infrastructure" in Japan.

[1] Y. Ono, Y. Hayashi, T. Ii, H. Tanabe, S. Ito, A. Kuwahata, T. Ito, Y. Kamino, T. Yamada, M. Inomoto and TS-Group, Phys. Plasmas **18**, 112113 (2011).
[2] Y. Ono, H. Tanabe, T. Yamada, M. Inomoto, T. Ii, S. Inoue, K. Gi, T. Watanabe, M. Gryaznevich, R. Scannell, C. Michael and C.Z. Cheng, Plasma Phys. Control. Fusion **54**, 124039 (2012).
[3] J. Yoo, M. Yamada, H. Ji, J. Jara-Almonte and C.E. Myers, Phys. Plasmas **21**, 055706 (2014).
[4] H. Tanabe, T. Yamada, T. Watanabe, K. Gi, M. Inomoto, R. Imazawa, M. Gryaznevich, C. Michael, B. Crowley, N.J. Conway, R. Scannell, J. Harrison, I. Fitzgerald, A. Meakins, N. Hawkes, K.G. McClements, T. O'Gorman, C.Z. Cheng, Y. Ono and MAST Team, Phys. Plasmas **24**, 056108 (2017).
[5] S. Usami, R. Horiuchi and H. Ohtani, Phys. Plasmas **24**, 092101 (2017).
[6] W. Pei, R. Horiuchi and T. Sato, Phys. Rev. Lett. **87**, 235003 (2001).
[7] H. Ohtani and R. Horiuchi, Plasma Fusion Res. **4**, 024 (2009).
[8] R. Horiuchi and T. Sato, Phys. Plasmas **4**, 277 (1997).
[9] X. Guo, R. Horiuchi, C. Z. Cheng, T. Kaminou and Y. Ono, Phys. Plasmas **24**, 032901 (2017).
[10] J.F. Drake, P.A. Cassak, M.A. Shay, M. Swisdak and E. Quataert, Astrophys. J. **700**, L16 (2009).
[11] C.Z. Cheng, S. Inoue, Y. Ono and R. Horiuchi, Phys. Plasmas **22**, 101205 (2015).
[12] R. Horiuchi and H. Ohtani, Comm. Comp. Phys. **4**, 496 (2008).